RAA 2016 Vol. **16** No. **9**, 138 (12pp) doi: 10.1088/1674–4527/16/9/138
http://www.raa-journal.org *http://iopscience.iop.org/raa*

***R**esearch in*
***A**stronomy and*
***A**strophysics*

A catalog of early-type emission-line stars and Hα line profiles from LAMOST DR2

Wen Hou[1,2], A-Li Luo[1,2], Jing-Yao Hu[1], Hai-Feng Yang[1,2,3], Chang-De Du[1,2], Chao Liu[1], Chien-De Lee[4], Chien-Cheng Lin[5], Yue-Fei Wang[6], Yong Zhang[6], Zi-Huang Cao[1] and Yong-Hui Hou[6]

[1] Key Laboratory of Optical Astronomy, National Astronomical Observatories, Chinese Academy of Sciences, Beijing 100012, China; *lal@bao.ac.cn, whou@bao.ac.cn*
[2] University of Chinese Academy of Sciences, Beijing 100049, China
[3] School of Computer Science and Technology, Taiyuan University of Science and Technology, Taiyuan 030024, China
[4] Institute of Astronomy, National Central University, Jhongli
[5] Shanghai Astronomical Observatory, Chinese Academy of Sciences, Shanghai 200030, China
[6] Nanjing Institute of Astronomical Optics & Technology, National Astronomical Observatories, Chinese Academy of Sciences, Nanjing 210042, China

Received 2015 December 3; accepted 2016 April 8

Abstract We present a catalog including 11 204 spectra of 10 436 early-type emission-line stars from LAMOST DR2, among which 9752 early-type emission-line spectra are newly discovered. For these early-type emission-line stars, we discuss the morphological and physical properties of their low-resolution spectra. In this spectral sample, the Hα emission profiles display a wide variety of shapes. Based on the Hα line profiles, these spectra are categorized into five distinct classes: single-peak emission, single-peak emission in absorption, double-peak emission, double-peak emission in absorption, and P-Cygni profiles. To better understand what causes the Hα line profiles, we divide these objects into four types from the perspective of physical classification, which include classical Be stars, Herbig Ae/Be stars, close binaries and spectra contaminated by H II regions. The majority of Herbig Ae/Be stars and classical Be stars are identified and separated using a (*H-K*, *K-W1*) color-color diagram. We also discuss 31 binary systems that are listed in the SIMBAD on-line catalog and identify 3600 spectra contaminated by H II regions after cross-matching with positions in the Dubout-Crillon catalog. A statistical analysis of line profiles versus classifications is then conducted in order to understand the distribution of Hα profiles for each type in our sample. Finally, we also provide a table of 172 spectra with Fe II emission lines and roughly calculate stellar wind velocities for seven spectra with P-Cygni profiles.

Key words: stars: early-type – stars: emission-line, Be — stars: pre-main sequence — binaries: close

1 INTRODUCTION

The strong optical emission lines which characterize hot emission-line stars enable the study of stellar envelopes, often revealing accretion flows, stellar winds and binary interaction. The objects with emission lines are widely distributed on the Hertzsprung-Russell diagram including various stellar types. Kogure & Leung (2007) divided the emission-line stars into four types, which are respectively early-type stars (Of, Oe/Be/Ae, etc), late type stars (dMe, Mira variables, etc), close binaries (Algol stars, cataclysmic variables and symbiotic stars), and pre-main sequence stars (Herbig Be/Ae stars and T Tauri stars). It is clear that the Hα emission line may be present in any of the early-type spectral classes. In general, the Hα emission stars with O, B or A spectral type are dominated by three types which are classical Be (Oe/Ae) stars (hereafter referred to as CBe stars), Herbig Ae/Be stars (hereafter HAeBe stars) and close binaries.

CBe stars are characterized by emission in Balmer lines, sometimes accompanied by emission in lines of singly-ionized metals or neutral helium (Kogure & Leung 2007; Gray & Corbally 2009). Jaschek et al. (1981) gave a more precise definition by segregating them as stars in luminosity classes V-III. Comprehensive reviews on the topic of CBe stars have been given in several works (Slettebak 1988; Porter & Rivinius 2003; Rivinius et al. 2013). Different from CBe stars, HAeBe stars are pre-main sequence stars with a mass of 2$\sim$10 $M_{\odot}$ (Waters & Waelkens 1998). Besides the emission lines of the Balmer series and some ionized metals such as Fe II, which exist in spectra of CBe stars, low-excitation lines such as Ca II

and Fe I also can be shown in the spectra of HAeBe stars. Properties that distinguish HAeBe from CBe stars are discussed in detail by Herbig (1960) and Strom et al. (1972). Many studies have also focused on the infrared (IR) color analysis of these two types, and distinguish them based on the IR excess in recent decades (Gehrz et al. 1974; Finkenzeller & Mundt 1984; Cote & Waters 1987; Hu & Xu 1990; Zhang et al. 2006; Lin et al. 2015). In addition to CBe and HAeBe stars, close binaries exhibiting both the Hα emission line and an early-type spectrum are usually comprised of Algol-type systems and cataclysmic variable stars such as novae (Kogure & Leung 2007).

It has been recognized that the Hα emission line in spectra originates from stellar envelopes or outer stellar atmospheres in early-type stars, due to the presence of strong stellar winds, rotating rings or accretion dust disks. Moreover, depending on the different physical mechanisms or the geometry of the objects, Hα emission profiles display a wide variety of shapes. Many attempts have already been made to investigate their physical origin, the Hα profile features and the classification of line profiles (Ulrich & Knapp 1979; Finkenzeller & Mundt 1984; Hanuschik et al. 1988; Reipurth et al. 1996; Reid & Parker 2012; Sigut & Patel 2013; Barnsley & Steele 2013; Bonito et al. 2013; Traven et al. 2015).

From previous studies, almost all the morphological classifications of Hα profiles are based on small samples of high-resolution spectra. In order to conduct an effective statistical analysis, we employ a total of $\sim$200 000 early-type stellar spectra acquired by the Large Sky Area Multi-Object Fiber Spectroscopic Telescope (LAMOST) survey until June 2014. From these observations we select a sample of 11 204 early-type emission-line spectra, representing 10 436 unique stars. Using these early-type Hα emission stars, we have analyzed two aspects of the Hα line profiles and physical classification.

In Section 2, we briefly describe the data and sample selection. A spectral analysis based on the Hα line profiles is presented in Section 3. We also give a detailed description of six morphological categories with additional unclassified profiles. In Section 4, a physical classification of these early-type Hα emission stars is provided. In Section 5, we analyze two particular classes: spectra with P-Cygni profiles and metal emission lines. Finally, a brief summary is provided in Section 6.

2 DATA AND SAMPLE SELECTION

2.1 The LAMOST Data

LAMOST, with an effective aperture of 4 m and a large field of view of 5°, is equipped with 16 spectrographs, 32 CCDs and 4000 fibers. A spectroscopic survey launched by this large instrument started in October 2011. It is planned to cover approximately half of the celestial sphere, and will eventually collect 10 million spectra of stars, galaxies and QSOs with a resolution of $\sim$1800 and a wavelength coverage of 3650–9000 Å. By June 2014, after completing the first-year pilot survey and first two years of the regular survey, more than 4 million spectra were observed, among which there were about 3.78 million stellar spectra. In the large dataset, $\sim$ 200 000 spectra, which account for about 5% of the stars in Data Release 2 (DR2), are classified as as O, B or A-type by the LAMOST 1D pipeline (Luo et al. 2015, 2016). A combined total of 200 259 O, B and A type stars are collected for H detection from DR2, among which the majority are A type stars.

2.2 Detection of the Hα Emission Line

In order to identify early-type stars with Hα in emission, we propose subjective criteria for detecting Hα line profiles. A brief description of the criteria is given here. For all the spectra of O, B and A-type stars, we use Equation (1) as the first criterion to select spectra with an Hα line in emission. This equation indicates that the average flux over the wavelength within five pixels of the Hα line center is larger than the continuum flux. This is useful for Hα emission lines with ordinary intensity above the continuum.

$$\sum_{i=-5}^{5} f_{\rm obs}[n_0 \, + \, i] \, / \, 11 \, > \, f_{\rm conti}[n_0] \, , \qquad (1)$$

where n_0 is the pixel index of the central wavelength of Hα (λ_0 = 6564 Å), and $f_{\rm obs}$ and $f_{\rm conti}$ denote the flux for observed spectra and continuum spectra respectively. A sample of 20 000 spectra is randomly selected from $\sim$ 200 000 O, B and A stars for testing Equation (1). Our manual checks confirmed that almost all the spectra with strong Hα emission lines can be picked out by using this equation, except for some spectra with weak emission lying in the deep Hα absorption profiles. To retrieve such spectra, we provide Equation (2) which can be applied to a narrow feature of Hα with fewer pixels, for detecting spectra with low-intensity Hα emission lines.

$$\sum_{i=-1}^{1} f[n_0+i]/3 > \sum_{i=-2}^{2} f[n_0+i]/5$$

and

$$\max\Big(f_{\rm obs}[n_0-1:n_0+1]\Big) \geqslant \max\Big(f_{\rm obs}[n_0-2:n_0+2]\Big) \qquad (2)$$

where the notations of n_0, $f_{\rm obs}$, $f_{\rm conti}$ are the same as in Equation (1), and $\max(f_{\rm obs}[x \, : \, y])$ represents the maximum flux where the index varies from x to y.

Applying these criteria to the initial sample, spectra satisfying either criterion are selected. It is noted that the noise in spectra may affect the selection of Hα emission lines, especially for spectra with a weak Hα emission line as well as a low signal to noise for the r band (SN_r$<$ 10). To be specific, detections of Hα emission lines are less accurate for spectra with lower SN_r. In order to ensure the results are as accurate as possible, we visually inspect all the selected spectra one by one, abandoning spectra with Hα profiles severely affected by noise. Finally,

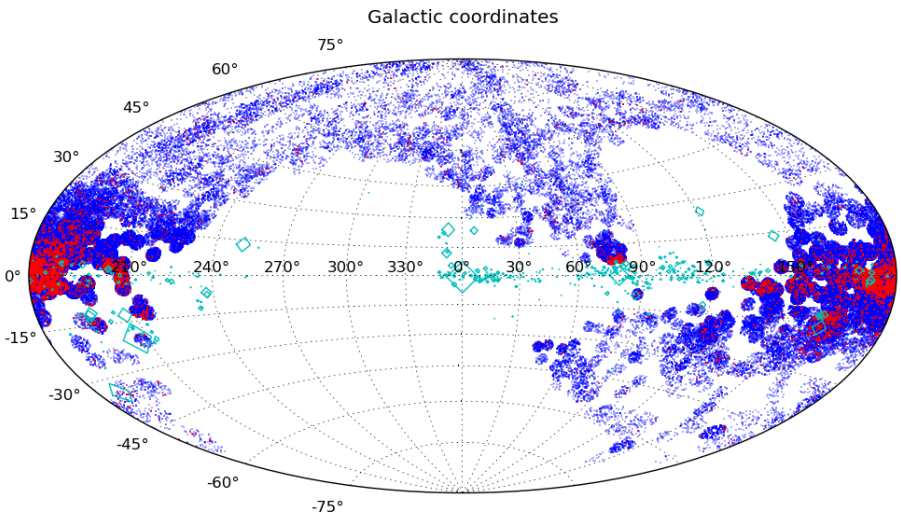

Fig. 1 The spatial distribution of both the initial sample and early-type Hα emission stars from LAMOST DR2. The blue and red points represent the combined sample of $\sim$ 200 000 O, B and A stars, and the 11 204 early-type Hα emission-line stars respectively. These two samples are concentrated in the region of the Galactic Anti-center due to the associated observational strategy. The cyan boxes represent H II regions which are discussed in Sect. 4.2.

Table 1 The Number of Spectra with Hα in Emission and the Total Number of Spectra for O, B and A Types

Spectral type	O type	B type	A type
Number of spectra with Hα emission lines	14	492	10 698
Total number of spectra	117	3137	197 005

a total of 11 204 spectra with Hα in emission is selected from LAMOST DR2. The spatial distribution of this sample in Galactic coordinates plotted by red points is shown in Figure 1. We can see that this sample is concentrated in the region of the Galactic Anti-center due to the associated observational strategy. The total number of spectra with Hα emission and the total number of stars for each spectral type are presented in Table 1.

3 MORPHOLOGICAL CLASSIFICATION OF Hα PROFILE

We endeavor to make a morphological classification of the Hα emission profile for the sample of low-resolution spectra. Quite similar to the classification system provided by Finkenzeller & Mundt (1984), here we divide the spectra in our sample into five morphological categories: emission with a single peak, emission with a single peak in absorption, emission with a double peak, emission with a double peak in absorption, and P-Cygni. The only difference between the first two categories is whether the emission lies in an apparent absorption component. This is also true for the third and the fourth cases. Five spectra (SN_r >50) with Hα emission profiles that are representative of the different types as well as one spectrum with an unclassified profile from the LAMOST survey are shown in Figure 2.

When making the morphological classification, it is noted that the shape of the Hα profile is probably affected by the SN_r of spectra. The classification results are more reliable for spectra with a high SN_r and vice-versa. Therefore, to incorporate reliability into the analysis, the dataset of spectra with Hα in emission from O, B and A-type stars in DR2 is divided into five groups based on SN_r which can indicate the noise level of the continuum around the Hα feature. These five groups are respectively subsamples with SN_r < 5, $5 \leq$ SN_r < 10, $10 \leq$ SN_r < 30, $30 \leq$ SN_r < 50 and SN_r ≥ 50.

Classification according to the shapes of Hα profiles for each group with different SN_r is made using the method of cross-correlation. The 27 templates used in the matching process contain five types of Hα profiles from single peak to P-Cygni with different intensities, which are visually chosen from spectra with SN_r higher than 50 in our sample. For a more accurate result, spectra for each type after template matching are also carefully inspected by eye. The statistical number of five groups corresponding to different categories as well as the group of unclassified profiles from low to high SN_r is presented in Figure 3. A detailed description of each type listed in this figure is given in the following, including the classification result and characteristics of each type of LAMOST spectrum.

(a) *single-peak profile (type I and type II)*: In our sample, single-peak profiles are comprised of type I and type II, which account for 5.45% and 73.7% respectively. Both types have emission lines with one peak, which are roughly symmetrical. The intensity of emission lines has a large span from tiny to large. Different from type I with only one emission line, type II is characterized by a single-peaked emission component su-

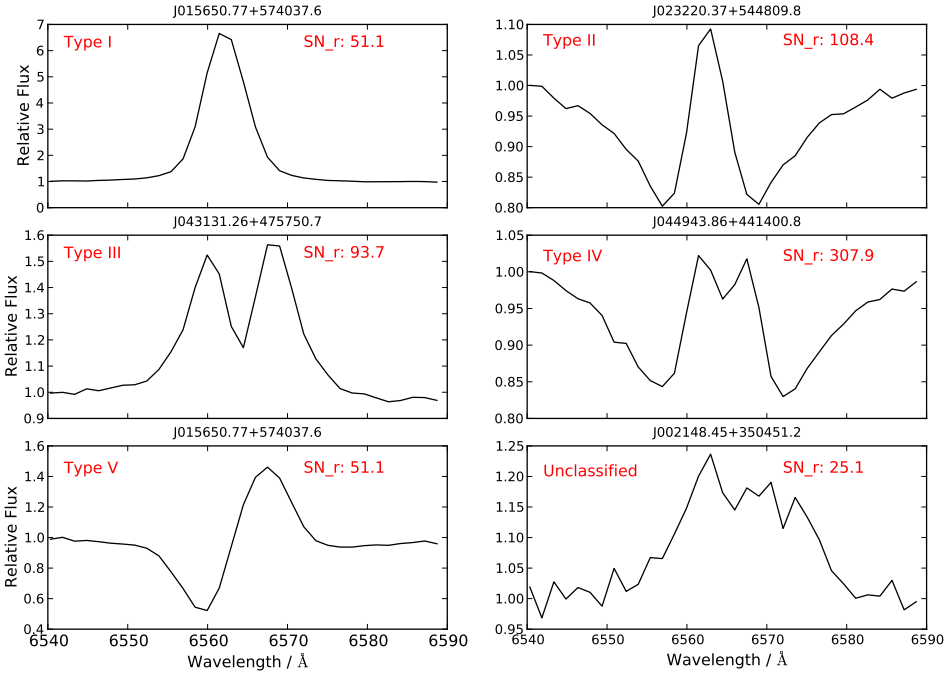

Fig. 2 Examples of six spectra with Hα emission lines that are representative of different types. These spectra with SN_r > 50 (except the unclassified one) are observed by the LAMOST facility with a resolution of $\sim$1800. Note: Radial velocities are not removed in these LAMOST spectra.

perimposed on a broad absorption component which originates from the photosphere of stars.

(b) *double-peak profile (type III and type IV)*: Double-peak profiles also include two types. Profiles of type III and type IV are observed in 1.35% and 6.35% of 11 204 Hα emission spectra, respectively. Similar to the first two types, the only difference is whether an additional broad underlying photospheric absorption exists in type III and type IV. These two types both contain two emission peaks separated by an absorption reversal which is approximately unshifted in most cases. The line profiles exhibit various structures, symmetric or asymmetric. Furthermore, a few spectra classified as type IV have quite a sharp and deep absorption component in the center of the double-peaked emission line, like in the spectra of Be shell stars.

(c) *P-Cygni profile (type V)*: A few spectra with P-Cygni profiles are also found in our sample. Out of 11 000 spectra, only seven show evident P-Cygni profiles, which are categorized as type V. From the appearance of the spectra, the P-Cygni profile has a blue absorption beyond the wing of the emission line. An accepted explanation of such P-Cygni profiles is that a gaseous envelope expands away from the star (Lamers 1998; Robinson 2007).

(d) *unclassified profile*: About 13.0 % of all the Hα emission spectra are placed in the group with unclassified profiles. This group is comprised of spectra with an Hα profile affected by noise or showing more complex shapes. Due to the limited resolving power of LAMOST instruments or disturbances from noise, an exact type cannot be given accurately. In addition, some spectra display more complex shapes of Hα profiles, such as a triple-peak profile which can be present in the spectra of a nova. However, profiles with more complex shapes can change over short periods. A detailed explanation of the formation can be found in Bianchini et al. (2004).

In summary, type II profiles are the most common in early-type Hα emission stars from our sample and account for the largest proportion of 73.7% seen from Figure 3. Moreover, a considerable number of spectra, about 13.0% percent of all the spectra, cannot be accurately classified into any of the five categories, which is probably caused by interference from noise on Hα profiles or more complex shapes of the Hα line. These spectra are considered as an individual unclassified group. Finally, we point out that the categories are just based on spectra with a resolution of $\sim$ 1800. Many of the single- and double-peak Hα profiles do not show microstructures due to the limited low resolution of spectra.

4 PHYSICAL CLASSIFICATION OF THE Hα EMISSION STARS

Various Hα emission profiles are produced by different physical mechanisms for different types of objects. In general, the Hα emission is always indicative of the existence of stellar envelopes, accretion or outflow activities in early-type emission-line stars. It is known that the Hα

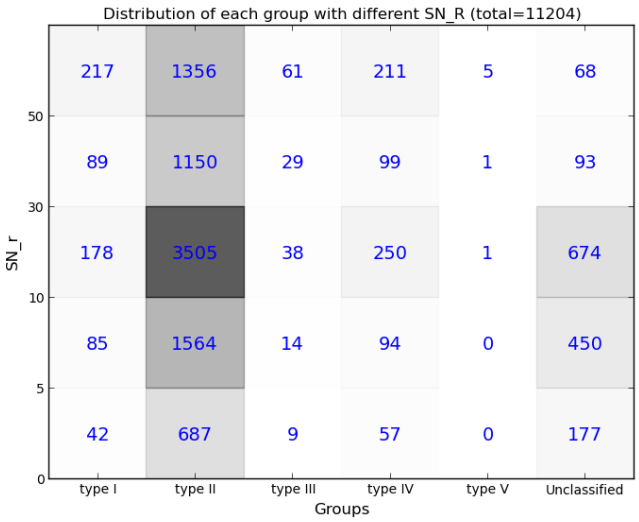

Fig. 3 The statistics of six groups with different SN_r. The x axis represents type I, type II, type III, type IV, type V and the unclassified profile from left to right respectively. The y axis represents five groups with different ranges of SN_r, which are <5, $5\sim10$, $10\sim30$, $30\sim50$ and ≥50 respectively. Each grid represents one type of SN_r in a certain range, and the number associated with each group is shown by the gray level of its grid.

emission line originates from the outer disks of CBe and HAeBe stars, and from the interactions of close binaries like the Algol system (Kogure & Leung 2007; Robinson 2007). The emission lines excited from the mechanisms mentioned above are all produced from stars. Moreover, there is one situation in which the Hα emission in a stellar spectrum may not be intrinsic. The emission lines can also originate from a diffuse nebula that is spread over the interstellar space. We provide a comprehensive analysis of our sample from the perspective of physical classification in the following subsections.

4.1 Objects Archived in Available Catalogs

In order to derive the number of newly discovered objects, it is necessary to verify how many known stars in our sample are recorded in previous literatures that describe our sample. Objects with definite categories compiled by SIMBAD and other catalogs are discussed in this section (Kohoutek & Wehmeyer 1999; Zhang et al. 2005; Witham et al. 2008; Neiner et al. 2011; Chojnowski et al. 2015; Lin et al. 2015).

By using the coordinates of objects, supplementary information on 1462 spectra are retrieved from the SIMBAD on-line database, for which a search radius of $3''$ is applied. By scanning the matching results, we find that about 1300 stars are flagged as "star" or "emission-line star" without more detailed object type in the SIMBAD database. The remaining stars with given classifications cover a variety of object types.

Among these objects, it is specifically noted that seven are CBe stars, three are HAeBe stars and 31 are close binaries in our sample. In addition, there are a small number of stars labeled as white dwarf or white dwarf candidates, supergiant stars or horizontal branch stars. In the classification of objects in our sample, the highest priority is given to the results from SIMBAD.

Table 2 The Number of Known Stars by Cross-matching Our Sample with Six Other Catalogs

Object type	Number	Reference
CBe stars	10	Neiner et al. (2011)
CBe stars	11	Chojnowski et al. (2015)
CBe stars	161	Lin et al. (2015)
CBe stars	4	Zhang et al. (2005)
Hα emission stars	74	Kohoutek & Wehmeyer (1999)
Hα emission stars	122	Witham et al. (2008)

In addition, several catalogs related to CBe stars, HAeBe stars or Hα emission stars have been published in recent years (Kohoutek & Wehmeyer 1999; Zhang et al. 2005; Witham et al. 2008; Neiner et al. 2011; Chojnowski et al. 2015; Raddi et al. 2015; Lin et al. 2015). We also cross-match our sample with these catalogs to select the known CBe and HAeBe stars. Moreover, there are 196 Hα emission stars that do not have a more detailed spectral type which has been compiled in other catalogs.

Table 2 presents the total number of stars cross-matched with existing catalogs.

4.2 Spectra Contaminated by H II Regions

Within our sample, there are some spectra which may be contaminated by H II regions. In such cases it is difficult to determine if the emission is intrinsic or extrinsic to the star itself. Therefore, we select all the stars whose coordinates are located in H II regions as an individual group by cross-matching with the catalog provided by Dubout-Crillon (as shown in Fig. 1).

There are some spectra that should be excluded from this group although they are projected int o H II regions. One case is the stars recorded as emission-line stars by the SIMBAD on-line catalog. The other case is the spectra which exhibit ionized iron emission lines originating from stars rather than H II regions. Finally, 3600 spectra are categorized as the group of spectra contaminated by H II regions.

4.3 Close Binaries

The interaction among close binaries is one of the formation mechanisms for the Hα emission line. Since sufficient information cannot be extracted from the spectra for identification, we only identify close binaries by cross-matching with the SIMBAD on-line catalog. SIMBAD lists 31 close binaries from our sample, which is comprised of 19 eclipsing binaries and 12 cataclysmic variable stars (two dwarf novae, three novae, two nova-like stars and five without subtypes).

4.4 CBe and HAeBe Stars

Apart from ordinary stars and those stars whose spectra are contaminated by H II regions, the remainder are predominately CBe and HAeBe stars. In order to distinguish these two types of stars, Finkenzeller & Mundt (1984) proposed a good criterion using a (*H-K*, *K-L*) diagram on the basis of much stronger IR excesses in HAeBe than in CBe stars. However, since observations in the *L* band are not only lacking but also not deep enough, it is reasonable to replace the *L* band by *W1*, the first band of *WISE* (Wright et al. 2010), in the color-color diagram for a large dataset. The magnitudes of *H* and *K* are collected from 2MASS (Skrutskie et al. 2006) and UKIDSS (Dye et al. 2006). Altogether, 6330 out of 7480 spectra simultaneously have *H*, *K* and *W1* available.

4.4.1 The analysis of photometric systems

The systematic errors between 2MASS and UKIDSS. Since the magnitudes of *H* and *K* bands are retrieved from 2MASS and UKIDSS, we analyze the systematic errors between these two *JHK* systems. We compare the color (*H-K*) and the magnitude of *K* band between 2MASS and UKIDSS which are applied in the color-color diagram. Because the number of common objects in both UKIDSS and 2MASS is quite small in our sample, we obtain the magnitudes of UKIDSS transformed from 2MASS through an empirical formula derived by Dye et al. (2006). The residual of (*H-K*) between two systems is 0.02 mag which is comparable to the observational uncertainty of 2MASS, and the residual of K magnitude is 0.005 mag which can be regarded as negligible. Since these residuals have a small effect on the classification of objects in the (*H-K*, *K-L*) diagram, the IR data from 2MASS in combination with UKIDSS are used without any calibrations.

We also consider the effect of replacing *L* with *W1* in the color-color criteria. In order to analyze the systematic error between *L* and *W1* magnitudes, we use 184 objects with measured *L* band magnitudes from Maercker & Burton (2005) and Maercker et al. (2006). A comparison reveals a mean difference of $\sim$0.1 mag with a standard deviation of $\sim \pm 0.2$ mag. The average reported observational accuracies for *L* and *W1* magnitudes are 0.06 ± 0.08 mag and 0.02 ± 0.03 mag respectively. This result indicates that the *W1* magnitude is basically consistent with the *L* magnitude. However, due to a lack of observations in the *L* band, the available samples are too few to provide an accurate calibration between *L* and *W1* bands. Despite this lack of calibration, the strong coincidence and low scatter between the two bands give us confidence in replacing *L* with *W1* in our color-color plot. Furthermore, we test the validity of (*K-W1*) color criteria by use of samples of known HAeBe and CBe stars. Using the *WISE W1* band magnitude for 40 HAeBe stars with *L* magnitude (Finkenzeller & Mundt 1984) and 122 CBe stars without *L* magnitude (Mathew & Subramaniam 2011), we plot the locations of these objects in the (*H-K*, *K-W1*) color-color diagram. The results show that only one HAeBe star and 13 CBe stars fall into the region in between. From this result, we conclude that the (*K-W1*) color-criteria can also separate HAeBe and CBe stars effectively, although a small fraction of the sample shows scatter between the regions of CBe stars and HAeBe stars.

4.4.2 Interstellar extinction correction

In the near IR region, extinction due to the interstellar medium along the line of sight to the star needs to be taken into account. Generally speaking, the interstellar extinction can be negligible for objects in high Galactic latitude areas ($b > 30^\circ$). However, for some objects in the low Galactic latitude areas, especially near the Galactic Anti-center, extinction is quite large. Therefore, the magnitudes of *H*, *K* and *W1* of low Galactic latitude objects are supposed to be corrected before using the color-color criterion. In the correction, we adopt $R_V = 3.1$ for $A_V = R_V \times E(B-V)$ (Schultz & Wiemer 1975; Hillenbrand et al. 1992; Zhang et al. 2006) and the extinction law A_λ/A_V from Yuan et al. (2013) where values of A_λ/A_V are 0.19, 0.13 and 0.082 for the *H*, *K* and *W1* bands respectively.

The color excess $E(B-V)$ of each object is obtained in two ways. 3925 spectra in our sample have the value of $E(B-V)$ with an accuracy of 0.04 mag retrieved from the LAMOST value-added catalog for LSS-GAC. For objects not found in the LAMOST value-added catalogs, $E(B-V)$ is estimated from $(B-V)$ – $(B-V)_0$. The observed color $(B-V)$ is taken from NOMAD (Zacharias et al. 2004) and the intrinsic color $(B-V)_0$ of stars for each spectral type is taken from Fitzgerald (1970). Although the maximum error of A_V is about 1 mag due to the uncertainty of spectral subtype determined by the LAMOST pipeline, it is acceptable for (*H–K*, *K–W1*) color-color classification (Finkenzeller & Mundt 1984). Finally, all the low

Galactic latitude stars with available magnitudes in *H*, *K* and *W1* are corrected for interstellar extinction according to the methods mentioned above.

4.4.3 Application of (H-K,K-W1) color-color criteria

Finkenzeller & Mundt (1984) pointed out that HAeBe stars typically occur in the region where $H\text{-}K > 0.4$ and $K\text{-}L > 0.8$, while CBe stars have $H\text{-}K < 0.2$ and $K\text{-}L < 0.5$. Before using these color criteria, the extinction corrections are applied to objects with low Galactic latitude as discussed above. Then we apply these criteria to our sample with *L* replaced by *W1*. All the objects which have available photometric data, de-reddened if necessary, have been placed in the *H-K*, *K-W1* color-color diagram, as shown in Figure 4. As a result, the large dataset is divided into three groups containing 23 HAeBe stars, 5594 CBe stars and 713 spectra in between. In 23 HAeBe stars, two objects have been investigated in the literature (Sartori et al. 2010; Kun et al. 2014), which are marked by open circles in Figure 4. For the objects scattered between the regions of CBe stars and HAeBe stars, we speculate that they are probably either CBe or HAeBe stars due to the uncertainty in IR color and the extinction correction. Additionally, it should be pointed out that B[e] stars may be also located in the region of HAeBe stars in the (*H-K*, *K-W1*) diagram, due to a large IR excess caused by hot circumstellar dust (Miroshnichenko 2006). Classification of these stars needs more information and further studies.

4.5 Analysis of the Hα Line Profiles According to Classifications

The mechanisms which give rise to Hα emission in CBe stars, HAeBe stars, close binaries and stars within H II regions can vary according to physical processes. Moreover, for a certain type of star, the shapes of Hα emission profiles can be caused by various physical processes. For investigating the distributions of different Hα profile shapes in each group, we perform a statistical analysis for the whole sample. The results are shown in Table 3 and Figure 5.

For CBe stars, as seen from the top-left panel of Figure 5, the shapes of Hα emission lines consist of single-peak, double-peak and P-Cygni profiles and they are dominated by type II (69.20%). A traditional and competitive explanation for the diversity in the line profile shapes is the different angles of the rotational axis of the star with respect to the observer's line-of-sight. Kogure & Leung (2007) have given a general description of various line profiles which may arise due to the inclination angle, which indicates double-peak profiles are the most prevalent among the spectra of CBe stars.

Similarly, all five types of Hα profiles are present in the spectra of HAeBe stars in our sample (the top-right panel of Fig. 5). A variety of theories have been proposed to interpret the Hα profiles with different shapes. For P-Cygni profiles, it is widely accepted that they originate in the stellar wind. Other profiles have been explained by several models, such as a clumpy circumstellar environment, magnetic models, winds with velocity gradients and rotation (Catala 1994; Reipurth et al. 1996).

Table 3 The Number of CBe, HAeBe Stars, Close Binaries and Objects Contaminated by H II Regions with Different Hα Profile Shapes

Type (1)	I (2)	II (3)	III (4)	IV (5)	V (6)	Unclassified (7)	Total (8)
CBe	272	3877	99	469	2	884	5603
HAeBe	8	10	1	4	1	2	26
close binaries	3	13	6	4	0	5	31
H II region	149	3079	16	131	0	225	3600

Columns (1)–(6): Types I to V represent single-peak emission, single-peak emission in absorption, double-peak emission, double-peak emission in absorption, and P-Cygni profiles respectively. Objects recorded by available catalogs are also added to each group which are presented in this table.

From Figure 5, we conclude that more than half of the profiles have a single peak in the low resolution spectra in our sample (R=1800), which is different from the sample from Finkenzeller & Mundt. Finkenzeller & Mundt (1984) made a comprehensive study of Hα profiles of 57 HAeBe stars or candidates using high-resolution spectra. They came to a conclusion that the double-peak profiles have the largest proportion, followed by single-peak and P-Cygni profiles. We infer that the overestimation of single-peak profiles and underestimation of double-peak profiles in both CBe and HAeBe stars of our sample probably result from the low resolution of spectra.

For close binaries and objects contaminated by H II regions, the relative fractions for each type of Hα profile are also shown in the bottom panels of Figure 5. No P-Cygni profiles (type V) are found in either group. Additionally, it is evident that the majority of spectra contaminated by H II regions show a single peak (the bottom-right panel of Figure 5).

4.6 Variability of Hα Profiles

There are some objects having more than one observation in our sample. In order to investigate the variability of the Hα emission profiles, we statistically analyze the frequency of multiple observations. The sample of Hα emission stars includes 11 204 spectra of 10 436 unique objects. A total of 9745 sources have been observed once, and 691 objects have repeated observations varying from two to six times. Then the equivalent widths of Hα lines are calculated for these stars with more than one spectrum. The information is listed in an individual table which is available on-line (*http://dr2.lamost.org/doc/vac*). In addition, we visually check all the spectra with repeated observations. It is found that $\sim$70% of the spectra display a stable Hα profile shape, and $\sim$30% exhibit an obvious change in the profile. There are two modes of Hα variability for the spectra in our sample, one of which is the change in emission line intensity and the other of which is the transformation be-

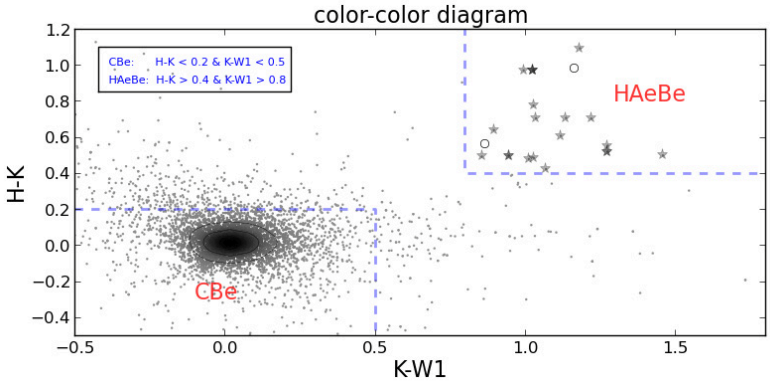

Fig. 4 The *H-K* vs. *K-W1* color-color diagram for 6330 early-type Hα emission stars from LAMOST DR2. The dashed lines represent the color criteria of CBe and HAeBe stars (Finkenzeller & Mundt 1984). 21 newly discovered HAeBe stars are plotted by star symbols, and two known stars are marked by open circles. The darker star symbols indicate multiple observations.

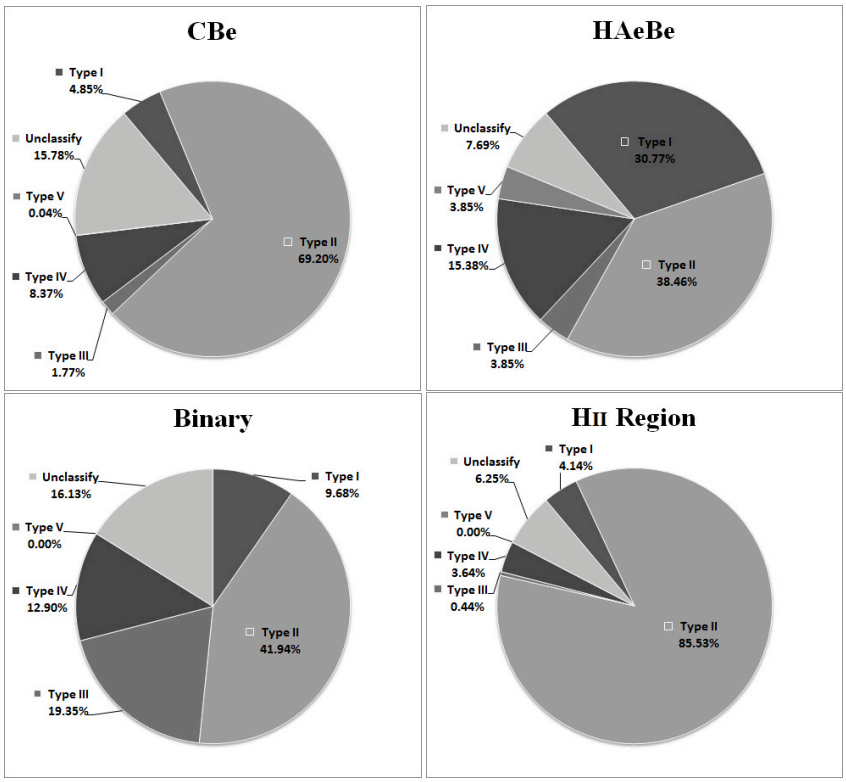

Fig. 5 The proportions of different Hα profile shapes are shown for CBe stars, HAeBe stars, close binaries and spectra contaminated by H II regions for the low resolution spectra in our sample ($R = 1800$).

tween two shapes such as the change from single-peak to double-peak profiles. Here, we need to point out that the times of observations and the quality of spectra play a key role in the reliability analysis of the Hα variability.

5 ANALYSIS OF THE SUBSAMPLES

5.1 A Subsample with Iron Emission Lines

In the sample of spectra with Hα emission from LAMOST DR2, the majority only display hydrogen emission, in most cases low order Balmer series such as the Hα or/and Hβ emission line. Sometimes, besides Balmer emission, metal emission, such as iron lines, is also present in a small number of spectra.

The study of Fe II emission lines, when measurable in Be stars, can contribute to understanding the physical properties of the circumstellar envelopes and the geometry of Be stars (Slettebak et al. 1992; Ballereau et al. 1995; Hanuschik 1994; Arias et al. 2006).

In order to obtain such a subsample displaying both Balmer and metal emission, we have detected three iron lines in the whole sample, including Fe II 5018 Å, 5169 Å and 5317 Å. Due to the weak intensity of iron lines,

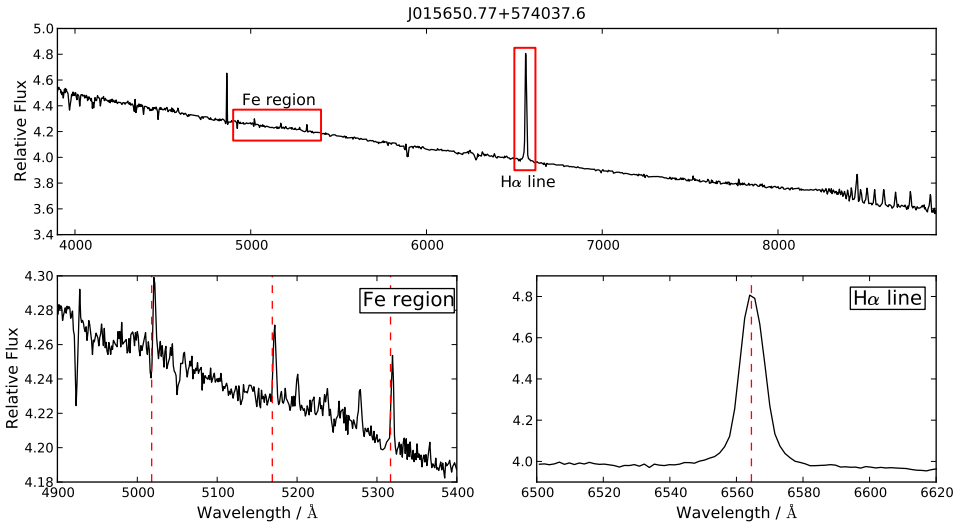

Fig. 6 Fe II emission lines with a single-peak. The spectrum with wavelength ranging from 3800 Å to 8900 Å is plotted in the *top* panel. Two regions of the spectrum are shown in the bottom panels, which are the features of Hα profile (*right*) and iron lines (*left*). Three lines of Fe II 5018 Å, 5169 Å and 5317 Å used in the emission detection are marked by the red dotted line in the *bottom-left* panel.

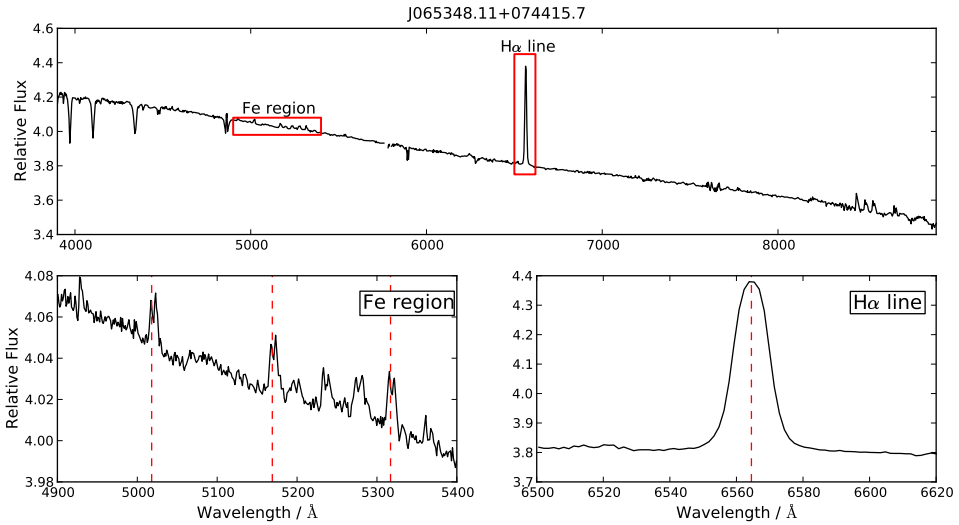

Fig. 7 Same as Fig. 6 but with Fe II emission lines showing a symmetric double-peak.

Table 4 The Basic Information on Seven Spectra with P-Cygni Profiles

Designation (1)	RA (2)	Dec (3)	$\lambda_{1\mathrm{blue}}$ (Å) (4)	$\lambda_{1\mathrm{red}}$ (Å) (5)	$\lambda_{2\mathrm{blue}}$ (Å) (6)	$\lambda_{2\mathrm{red}}$ (Å) (7)	V_{wind} (km s^{-1}) (8)
J035859.44+561112.6	59.747674	56.186845	6555.307108	6564.567527	4855.135384	4862.518663	439.35
J063115.43+313054.5	97.814293	31.515164	6558.924803	6564.867627	/	/	271.58
J063032.91+055217.8	97.637126	5.8716309	6560.106444	6566.502805	/	/	292.31
J063032.94+055211.5	97.637261	5.869869	/	/	4860.226369	4863.471923	200.23
J055054.77+201447.6	87.72822	20.246568	6563.579882	6566.432534	/	/	130.37
J034753.05+291200.0	56.971046	29.200009	6560.456203	6567.886835	/	/	339.58
J034753.05+291200.0	56.971046	29.200009	6560.746404	6568.088851	/	/	335.55

Notes: Columns (1)–(3): Designation, RA and Dec are retrieved from the LAMOST catalog; Cols. (4)–(7): $\lambda_{1\mathrm{blue}}$ and $\lambda_{1\mathrm{red}}$ are the wavelength centers for the absorption and emission components obtained by a fitting for Hα profiles; $\lambda_{2\mathrm{blue}}$ and $\lambda_{2\mathrm{red}}$ are for Hβ profiles. '/' in the table indicates the emission lines without an evident P-Cygni profile; Cols. (8): V_{wind} gives broad estimates for the stellar wind velocities.

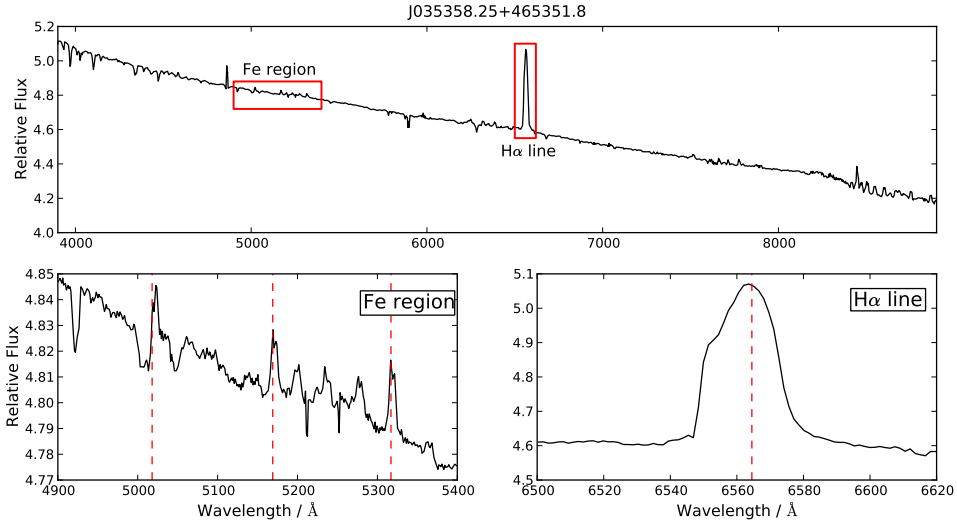

Fig. 8 Same as Fig. 6 but with Fe II emission lines showing an asymmetric double-peak.

which are easily disturbed by noise in early-type spectra, a dataset with signal to noise for the g band higher than 10 (SN_g$\geq$10) is chosen for detection of Fe II emission. 172 spectra that show both intense iron and Balmer emission have been selected from spectra with Hα emission lines. The profiles of iron emission lines also exhibit various types, including single-peak, double-peak (symmetric or asymmetric) and P-Cygni. Various types of metal line profiles are shown from Figure 6 to Figure 9. Besides Balmer and iron features, many other common emission lines are also found in these spectra, such as the O I, Ca II triplet or the Paschen series. A table of the 172 spectra with Fe II emission lines is provided online (*http://dr2.lamost.org/doc/vac*), which includes four columns with the headings of designation, RA, Dec and Fe_type. The first column represents the designation in LAMOST, the second and the third ones provide equatorial coordinates of the objects, and the last column signifies the morphological type of Fe II emission lines.

5.2 P-Cygni Profiles and Stellar Wind Velocity

Seven spectra having Hα emission showing a P-Cygni profile in five unique objects are discussed in this section. These profiles consist of a broad intense emission line with an absorption line displaced to the blue side of the emission component. It has been well known that such profiles indicate the existence of an outflowing wind in the neighborhood of the star. A detailed explanation of line formation and related physical processes has been given by Lamers (1998) and Robinson (2007). The basic information about the seven spectra is listed in Table 4. (The 3th and 4th cases are associated with the same star, as are the 6th and 7th cases.)

Specifically, the velocities of stellar wind for each object in the 8th column can be roughly derived from the Doppler effect formula

$$V_{\rm wind} = (\Delta\lambda/\lambda_0) \times c\,, \tag{3}$$

where $\Delta\lambda$ is the difference in wavelength between the center of the emission and the absorption component, λ_0 is the center of the rest wavelength for the corresponding feature band, and c is the speed of light. In order to obtain the difference in the center of wavelength between the two components ($\Delta\lambda$), we have fitted Hα or/and Hβ profiles of each spectrum by the combination of two independent Gaussian profiles representing emission and absorption lines, as well as a linear function representing the local continuum. The fitting function is defined as follows

$$f(x) = \sum_{i=1}^{2} A_i e^{-\frac{(x-\lambda_i)^2}{2\sigma_i^2}} + (ax+b) \tag{4}$$

where A_i, λ_i and σ_i represent the amplitude, the center and the standard deviation for the emission or absorption lines. Taking an Hα profile as an example, $\Delta\lambda_\alpha$ (i.e. λ_1-λ_2) can be derived by the Gaussian fitting using Equation (4). Then wind velocity v_α is calculated by simply plugging the difference of wavelength center $\Delta\lambda_\alpha$ into Equation (3). Applying this method to an Hβ profile, we can also measure the wind velocity v_β and the adopted wind velocity $V_{\rm wind}$ is the average of v_α and v_β. An example of spectral lines with a P-Cygni profile fitted by a double Gaussian function is shown in Figure 10.

6 SUMMARY

We provide a catalog including 11 204 spectra for 10 436 early-type emission-line stars from LAMOST DR2, among which 9752 early-type emission-line spectra are newly discovered. The catalog can be accessed at the LAMOST Data Release web portal,

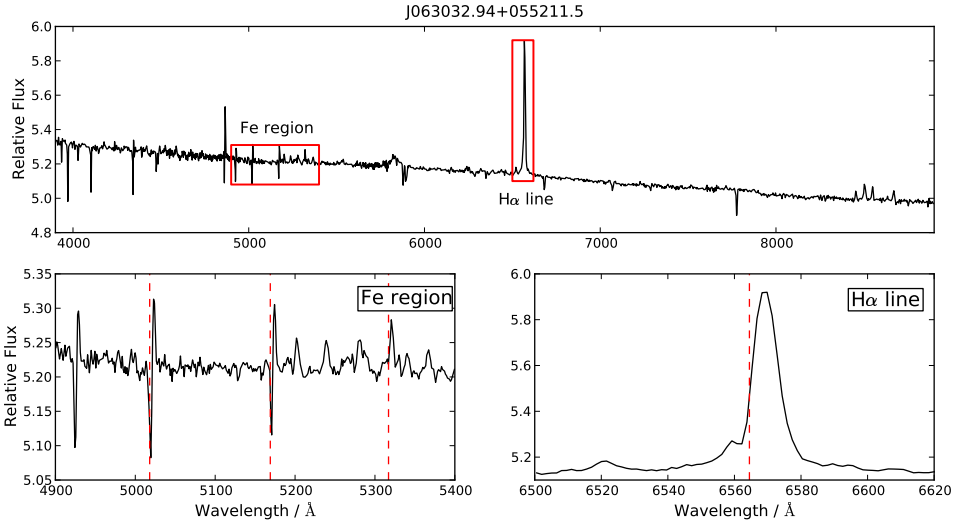

Fig. 9 Same as Fig. 6 but with Fe II emission lines showing P-Cygni profiles.

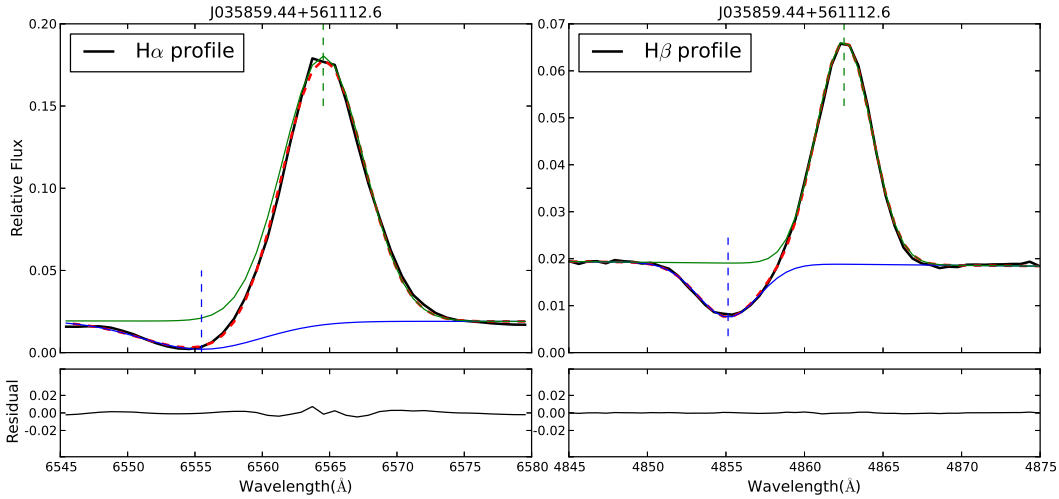

Fig. 10 An example of the P-Cygni profiles of Hα and Hβ lines fitted by double-Gaussian functions. In the *top* panels, the black line represents the Hα profile of the observational spectrum and the red dashed line is the result of double-Gaussian fitting. The blue and green dashed lines represent the fitting results of absorption and emission component respectively. The residuals for the fitting are plotted in the *bottom* panels.

http://dr2.lamost.org/doc/vac. It consists of 12 columns, which are respectively the designation in LAMOST, coordinates (RA and Dec), *W1* magnitude and the error, *H* magnitude and the error, *K* magnitude and the error, morphological type of Hα profiles, and object types classified by our criteria and SIMBAD.

We also perform a spectral analysis of the 11 204 spectra from LAMOST DR2. According to the Hα line profiles, these spectra are classified into five distinct classes as well as a group of unclassified profiles. Moreover, four types of objects are found in our sample including CBe stars, HAeBe stars, close binaries and spectra contaminated by H II regions. Analyses of P-Cygni profiles and ionized iron emission lines are also included in this paper. Our analyses are based on a large sample of spectra with low resolution. More sophisticated studies of interesting spectra need more information such as high-resolution spectra from follow-up observations. The data of LAMOST DR2 can be downloaded (*http://dr2.lamost.org*) to international researchers after the formal data release in June 2016.

Acknowledgements We thank the anonymous referees for constructive comments. This work is supported by the National Key Basic Research Program of China (Grant No. 2014CB845700), and the National Natural Science Foundation of China (Grant Nos. 11390371 and 11233004).

The Guo Shou Jing Telescope (the Large Sky Area Multi-Object Fiber Spectroscopic Telescope, LAMOST) is a National Major Scientific Project built by the Chinese Academy of Sciences. Funding for the project has been provided by the National Development and Reform Commission. LAMOST is operated and managed by National Astronomical Observatories, Chinese Academy of Sciences. In addition, we also thank C. Neiner for providing the BeSS catalog.

References

Arias, M. L., Zorec, J., Cidale, L., et al. 2006, A&A, 460, 821
Ballereau, D., Chauville, J., & Zorec, J. 1995, A&AS, 111, 457
Barnsley, R. M., & Steele, I. A. 2013, A&A, 556, A81
Bianchini, A., Mastrantonio, E., Canterna, R., Stute, J., & Cantrell, K. 2004, A&A, 426, 669
Bonito, R., Prisinzano, L., Guarcello, M. G., & Micela, G. 2013, A&A, 556, A108
Catala, C. 1994, in Astronomical Society of the Pacific Conference Series, 62, The Nature and Evolutionary Status of Herbig Ae/Be Stars, eds. P. S. The, M. R. Perez, & E. P. J. van den Heuvel, 91
Chojnowski, S. D., Whelan, D. G., Wisniewski, J. P., et al. 2015, AJ, 149, 7
Cote, J., & Waters, L. B. F. M. 1987, A&A, 176, 93
Dubout-Crillon, R. 1976, A&AS, 25, 25
Dye, S., Warren, S. J., Hambly, N. C., et al. 2006, MNRAS, 372, 1227
Finkenzeller, U., & Mundt, R. 1984, A&AS, 55, 109
Fitzgerald, M. P. 1970, A&A, 4, 234
Gehrz, R. D., Hackwell, J. A., & Jones, T. W. 1974, ApJ, 191, 675
Gray, R. O., & Corbally, J., C. 2009, Stellar Spectral Classification (Princeton Univ. Press)
Hanuschik, R. W. 1994, in IAU Symposium, 162, Pulsation; Rotation; and Mass Loss in Early-Type Stars, eds. L. A. Balona, H. F. Henrichs, & J. M. Le Contel, 265
Hanuschik, R. W., Kozok, J. R., & Kaiser, D. 1988, A&A, 189, 147
Herbig, G. H. 1960, ApJS, 4, 337
Hillenbrand, L. A., Strom, S. E., Vrba, F. J., & Keene, J. 1992, ApJ, 397, 613
Hu, J.-Y., & Xu, Z. 1990, Acta Astrophysica Sinica, 10, 154
Jaschek, M., Slettebak, A., & Jaschek, C. 1981, Be star terminology., Be Star Newsletter, 4, 9
Kogure, T., & Leung, K.-C., eds. 2007, Astrophysics and Space Science Library, 342, The Astrophysics of Emission-Line Stars
Kohoutek, L., & Wehmeyer, R. 1999, A&AS, 134, 255
Kun, M., Racz, M., & Szabados, L. 2014, Information Bulletin on Variables, 6089, 1
Lamers, H. J. G. L. M. 1998, Ap&SS, 260, 63
Lin, C.-C., Hou, J.-L., Chen, L., et al. 2015, RAA (Research in Astronomy and Astrophysics), 15, 1325
Luo, A.-L., Zhao, Y.-H., Zhao, G., et al. 2016, submitted
Luo, A.-L., Zhao, Y.-H., Zhao, G., et al. 2015, RAA (Research in Astronomy and Astrophysics), 15, 1095
Maercker, M., & Burton, M. G. 2005, A&A, 438, 663
Maercker, M., Burton, M. G., & Wright, C. M. 2006, A&A, 450, 253
Mathew, B., & Subramaniam, A. 2011, Bulletin of the Astronomical Society of India, 39, 517
Miroshnichenko, A. S. 2006, in Astronomical Society of the Pacific Conference Series, 355, Stars with the B[e] Phenomenon, eds. M. Kraus, & A. S. Miroshnichenko, 13
Neiner, C., de Batz, B., Cochard, F., et al. 2011, AJ, 142, 149
Porter, J. M., & Rivinius, T. 2003, PASP, 115, 1153
Raddi, R., Drew, J. E., Steeghs, D., et al. 2015, MNRAS, 446, 274
Reid, W. A., & Parker, Q. A. 2012, MNRAS, 425, 355
Reipurth, B., Pedrosa, A., & Lago, M. T. V. T. 1996, A&AS, 120, 229
Rivinius, T., Carciofi, A. C., & Martayan, C. 2013, A&A Rev., 21, 69
Robinson, K. 2007, Spectroscopy: The Key to the Stars (Springer)
Sartori, M. J., Gregorio-Hetem, J., Rodrigues, C. V., Hetem, Jr., A., & Batalha, C. 2010, AJ, 139, 27
Schultz, G. V., & Wiemer, W. 1975, A&A, 43, 133
Sigut, T. A. A., & Patel, P. 2013, ApJ, 765, 41
Skrutskie, M. F., Cutri, R. M., Stiening, R., et al. 2006, AJ, 131, 1163
Slettebak, A. 1988, PASP, 100, 770
Slettebak, A., Collins, II, G. W., & Truax, R. 1992, ApJS, 81, 335
Strom, S. E., Strom, K. M., Yost, J., Carrasco, L., & Grasdalen, G. 1972, ApJ, 173, 353
Traven, G., Zwitter, T., Van Eck, S., et al. 2015, A&A, 581, A52
Ulrich, R. K., & Knapp, G. R. 1979, ApJ, 230, L99
Waters, L. B. F. M., & Waelkens, C. 1998, ARA&A, 36, 233
Witham, A. R., Knigge, C., Drew, J. E., et al. 2008, MNRAS, 384, 1277
Wright, E. L., Eisenhardt, P. R. M., Mainzer, A. K., et al. 2010, AJ, 140, 1868
Xiang, M., et al. 2015, in prep.
Yuan, H. B., Liu, X. W., & Xiang, M. S. 2013, MNRAS, 430, 2188
Yuan, H.-B., Liu, X.-W., Huo, Z.-Y., et al. 2015, MNRAS, 448, 855
Zacharias, N., Monet, D. G., Levine, S. E., et al. 2004, in Bulletin of the American Astronomical Society, 36, American Astronomical Society Meeting Abstracts, 1418
Zhang, P., Chen, P. S., & Yang, H. T. 2005, New Astron., 10, 325
Zhang, P., Yang, H. T., & Liu, J. 2006, Ap&SS, 305, 11